

Article

# Hydrogenative Cyclization of Levulinic Acid to $\gamma$ -Valerolactone with Methanol and Ni-Fe Bimetallic Catalysts

Ligang Luo <sup>1,\*</sup>, Xiao Han <sup>1,†</sup> and Qin Zeng <sup>1,2</sup>

<sup>1</sup> College of Life Science, Shanghai Normal University, 100 Guilin Rd, Shanghai 200241, China; wo.lixiang0530@163.com (X.H.); zengqllg@usst.edu.cn (Q.Z.)

<sup>2</sup> The Public Experiment Center, University of Shanghai for Science and Technology, Shanghai 200093, China

\* Correspondence: ligangluo@shnu.edu.cn

† Ligang Luo and Xiao Han Contributed equally to this work.

Received: 26 August 2020; Accepted: 14 September 2020; Published: 21 September 2020



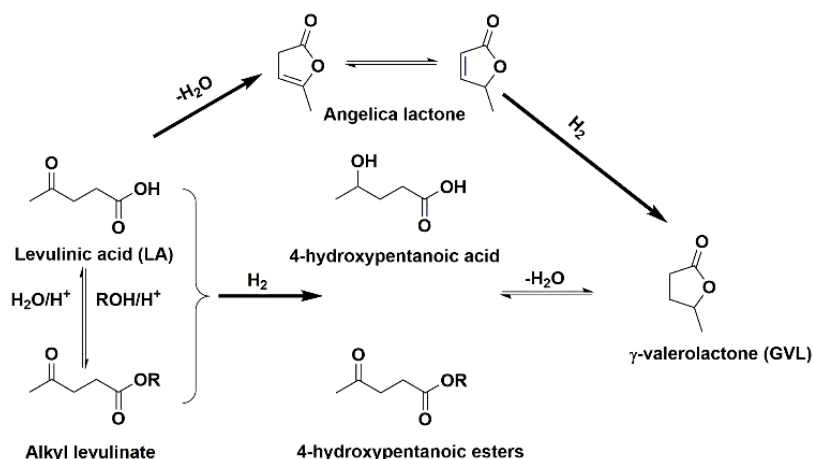
**Abstract:** A series of Ni-Fe/SBA-15 catalysts was prepared and tested for the catalytic hydrogenation of levulinic acid to  $\gamma$ -valerolactone, adopting methanol as the only hydrogen donor, and investigating the synergism between Fe and Ni, both supported on SBA-15, towards this reaction. The characterization of the synthesized catalysts was carried out by XRD (X-ray powder diffraction), TEM (transmission electron microscopy), H<sub>2</sub>-TPD (hydrogen temperature-programmed desorption), XPS (X-ray photoelectron spectroscopy), and in situ FT-IR (Fourier transform–infrared spectroscopy) techniques. H<sub>2</sub>-TPD and XPS results have shown that electron transfer occurs from Fe to Ni, which is helpful both for the activation of the C=O bond and for the dissociative activation of H<sub>2</sub> molecules, also in agreement with the results of the in situ FT-IR spectroscopy. The effect of temperature and reaction time on  $\gamma$ -valerolactone production was also investigated, identifying the best reaction conditions at 200 °C and 180 min, allowing for the complete conversion of levulinic acid and the complete selectivity to  $\gamma$ -valerolactone. Moreover, methanol was identified as an efficient hydrogen donor, if used in combination with the Ni-Fe/SBA-15 catalyst. The obtained results are promising, especially if compared with those obtained with the traditional and more expensive molecular hydrogen and noble-based catalysts.

**Keywords:** biomass ester derivatives; solvothermal processing; levulinic acid;  $\gamma$ -valerolactone; Ni-Fe bimetallic catalysts

## 1. Introduction

The world is highly dependent on the utilization of fossil resources to fulfill energy needs for the production of heat and power. Nevertheless, the surplus consumption of fossil fuels is escalating the concentration of atmospheric CO<sub>2</sub>, which causes serious global warming threats [1,2]. As a solution to the above primary challenges, considerable attention has been paid to the exploitation of renewable resources [1]. In this context, the conversion of the cellulose fraction of biomass into value-added platform chemicals, such as 5-hydroxymethylfurfural (5-HMF) and levulinic acid (LA), has been thoroughly investigated [2,3]. Moreover, the transformation of LA into more added-value bio-fuels and bio-chemicals is strategic, thanks to its reactive keto and carboxylic functional groups, which can be exploited for the synthesis of many valuable bio-chemicals, such as fuel additives, fragrances, solvents, pharmaceuticals, and plasticizers [4]. Among these high-value chemicals,  $\gamma$ -valerolactone (GVL) is receiving considerable attention to synthesize added-value bio-chemicals, such as food additives, solvents, and drug intermediates, as well as new bio-fuels [5,6]. Three pathways have been proposed

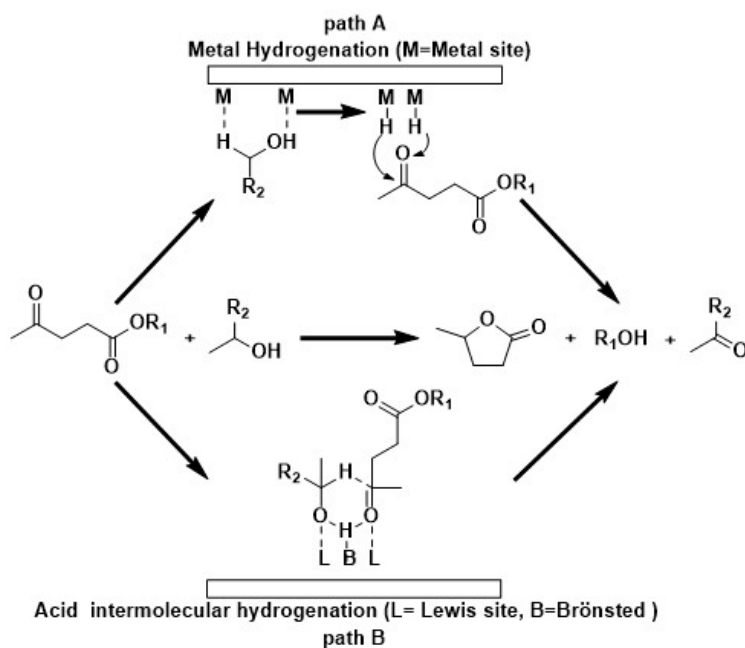
for GVL production, as reported in Scheme 1. The first requires the high-temperature LA conversion in the gas phase, occurring via its endothermic dehydration to angelicalactone, which is subsequently hydrogenated to GVL. The second occurs in the liquid phase, at lower temperatures, where the LA keto group is reduced to 4-hydroxyvaleric acid, which is in turn dehydrated to GVL. Lastly, the third possibility provides the esterification of LA to the less reactive alkyl levulinate, which undergoes hydrogenation and dehydration to GVL [6].



**Scheme 1.** Different pathways for the hydrogenation of levulinic acid (LA) to  $\gamma$ -valerolactone (GVL).

According to the above mechanisms, dehydration is generally favored by the presence of acid catalysts, whereas the hydrogenation is catalyzed by transition metals. Many homogeneous and heterogeneous catalysts have been employed for the hydrogenation of LA to GVL in the liquid phase [7]. However, given the well-known drawbacks of the homogeneous catalysts (the possible corrosion of the equipment, difficult recycle/reuse, and environmental concerns), heterogeneous ones have been certainly preferred [8]. Many noble metal catalysts have been tested for this reaction, in particular, Pt, Au, Pd, Rh, and Ru, in many cases achieving promising catalytic performances with respect to GVL [9–12]. For example, Son et al. have studied the catalytic performances of Ru/C, Ru/SBA, Au/ZrC, and Au/ZrO<sub>2</sub> catalysts for the LA hydrogenation, highlighting the good catalytic performances and stability of the Au/ZrO<sub>2</sub> catalyst, which can be reused five times, achieving a high GVL yield (90 mol %) [10]. However, although the noble metal catalysts show excellent performances for the hydrogenation of such carbonyl compounds, the high costs limit their further application in the industry. On this basis, non-noble metal catalysts remain the preferred choice for improving the sustainable catalytic transformation of LA to GVL [13,14]. In particular, Ni-based catalysts (Raney-Ni, Ni/MoO<sub>x</sub>/C, Cu/ZrO<sub>2</sub>, NiCu/Al<sub>2</sub>O<sub>3</sub>, and Mo<sub>2</sub>C) are active in this reaction [13–15]. For example, Mohan et al. have examined the influence of catalysts with Ni supported on SiO<sub>2</sub>, Al<sub>2</sub>O<sub>3</sub>, ZnO, ZrO<sub>2</sub>, TiO<sub>2</sub>, and MgO, highlighting the excellent catalytic performances of Ni/SiO<sub>2</sub> towards the LA hydrogenation to GVL (0.8506 kg GVL kg catalyst<sup>-1</sup> h<sup>-1</sup> at 250 °C) [15]. The characterization of these catalysts by FT-IR spectroscopy has indicated that both Lewis and Brønsted acid sites play an important role in the dehydration of the intermediate 4-hydroxypentanoic acid [16], thus highlighting that the use of tunable bifunctional catalysts is preferred for improving the catalysis of this reaction. In this context, the addition of another metal could modify the electronic structure of Ni, decreasing the interaction between active metal and supports, thus enhancing the reaction activity [17]. For example, the Cu species had an important effect on the chemical environment of Ni species and acted as an electronic promoter on Ni surface active sites in Ni-Cu/Al<sub>2</sub>O<sub>3</sub> bimetallic catalysts, achieving the highest GVL yield of 96 mol % (250 °C, 6.5 MPa, and 2 h) [18]. Regarding the possible hydrogen sources, LA hydrogenation has been carried out mainly with molecular H<sub>2</sub> (0.8–6.5 MPa), both in batch autoclaves and in continuous flow reactors, generally obtaining high yields and selectivities to GVL [15–17]. However, this reaction requires large quantities of molecular H<sub>2</sub>, whose production

is still mostly fossil based, which also raises cost and safety issues. In this context, formic acid and alcohols have been proposed as alternative hydrogen donors, which should help one to avoid the usage of external  $H_2$  and, subsequently, the requirement for a high-pressure reactor [19]. Regarding formic acid,  $H_2$  is generated through the decarboxylation route ( $HCOOH \rightarrow CO_2 + H_2$ ), which is generally slow, unless noble metals, such as Ru, are used as catalysts [19,20]. However, Ruppert et al. have demonstrated that formic acid can be irreversibly adsorbed on the Ru/C catalyst, hampering the LA conversion to GVL [21]. Furthermore, agglomeration and metal leaching generally occur, which could greatly affect catalyst stability, thus significantly hampering its effective use [22]. Alternatively, it is possible to use alcohol as an  $H_2$  source, and perform a hydrogen transfer, which is known as the Meerwein–Ponndorf–Verley (MPV) reaction, which is catalyzed by Lewis acid sites, such as those of metal oxides or zeolites [23]. Two mechanisms have been proposed for explaining the hydrogen transfer in the presence of alcohols, both reported in Scheme 2 [23–25]. In the first one (path A, Scheme 2), the MPV reaction is catalyzed by the metal catalyst, which receives the hydrogen from the alcohol donor, through  $\beta$ -hydride elimination, and the activated hydrogen is then transferred from the metal to the acceptor molecule, in this case LA [24]. The second one involves an intermolecular hydrogen transfer, which occurs by adsorption of the hydroxyl group of the alcohol and the carbonyl group of LA (or its ester) on the catalyst surface [25]. This direct reaction is allowed thanks to the presence of Lewis and Brønsted acids, both leading to the formation of a six-membered ring transition state. Luo et al. have studied the MPV reaction of methyl levulinate to GVL in the presence of zeolites, confirming that the main rate-limiting step of this reaction is the hydride shift [25].



**Scheme 2.** Catalytic transfer hydrogenation mechanisms of LA.

Many kinds of alcohol have been employed for the MPV reaction, highlighting the higher reaction rates of the secondary alcohols. Chia et al. employed 2-BuOH to study the MPV transfer hydrogenation, achieving a good GVL yield (84.7 mol %), over the  $ZrO_2$  catalyst (150 °C, 16 h) [24]. A strong correlation has been established between the reducing capacity of alcohols and MPV reduction, according to this order: MeOH < EtOH < 1-BuOH < 2-BuOH = 2-PrOH [26]. However, by using MeOH or EtOH as hydrogen donors, more efficient and integrated biomass utilization chains could be created, thanks to the high availability of these alcohols from biomass feedstock. Tang et al. have used EtOH as a hydrogen donor, achieving the maximum GVL yield of 64 mol % (250 °C, 3 h) [26]. Yi et al. have reported that no hydrogen transfer observed within 48 h in the presence of EtOH, whilst a GVL yield of 38 mol % was achieved with 1 MPa  $H_2$ , after only 2 h [27]. Despite the achieved progress, it is definitely

still necessary to develop new, efficient and cheap catalytic systems for the LA hydrogenation to GVL, by MPV catalytic transfer, in the presence of short-chain primary alcohols.

In this work, new bimetallic Ni-Fe/SBA-15 catalysts have been synthesized and tested for the LA hydrogenation to GVL by the MPV route, in the presence of MeOH as the only hydrogen donor, and the oxophilic promotion of Fe was exploited to decrease the reduction temperature of the NiO phase and improve the reducibility of mixed oxides. Ni, Fe, and bimetallic Ni-Fe catalysts with different Fe/Ni molar ratios have been prepared by impregnation on the SBA-15 support, which helps the LA conversion to GVL. Moreover, this support provides high specific surface area (ranging between 690 and 1040 m<sup>2</sup>/g), narrow pore size distribution (average pore diameter between 5 and 30 nm), and high thermal stability (wall thicknesses between 3 and 5 nm) [28,29]. To investigate the relationship between catalyst structure and activity, characterization of the bimetallic Ni-Fe catalysts was performed by X-ray powder diffraction (XRD), transmission electron microscopy (TEM), hydrogen temperature-programmed desorption (H<sub>2</sub>-TPD), hydrogen temperature-programmed reduction (H<sub>2</sub>-TPR), X-ray photoelectron spectroscopy (XPS), and in situ Fourier transform-infrared spectroscopy (FT-IR). Lastly, the effects of the main reaction parameters on the GVL production have been evaluated and discussed, starting from the results of preliminary catalytic tests.

## 2. Results and Discussion

### 2.1. Characterization of Catalysts

First, the catalysts have been characterized by the XRD technique to investigate the atomic structure of the particles (Figure 1). The XRD patterns of Ni/SBA-15 catalyst exhibit three diffraction peaks at  $2\theta$  values of 44.2°, 51.8°, and 76.3°, which are assigned to (111), (200), and (220) reflections of metallic Ni, respectively. Fu et al. reported analogous diffraction peaks for the Ni/Al<sub>2</sub>O<sub>3</sub> catalyst at  $2\theta$  angles of 44.3°, 51.7°, and 76.3°, assigned to metallic Ni [15]. Nevertheless, the absence of the diffraction peak at 37.3°, due to the NiO species, confirms the complete reduction of the Ni particles [15]. In the case of the monometallic Fe/SBA-15 catalyst, another diffraction peak was found at about 44.7°, which can be assigned to the (111) Fe cubic planes [30]. However, in the case of the Ni-Fe/SBA-15 catalysts, the Fe peak is shifted to lower  $2\theta$ , indicating a deep interaction between Ni and Fe particles to form face-centered cubic structures (fcc) of the Ni-Fe alloy, favored by the larger atomic radius of Fe, which increases the lattice constants [16].

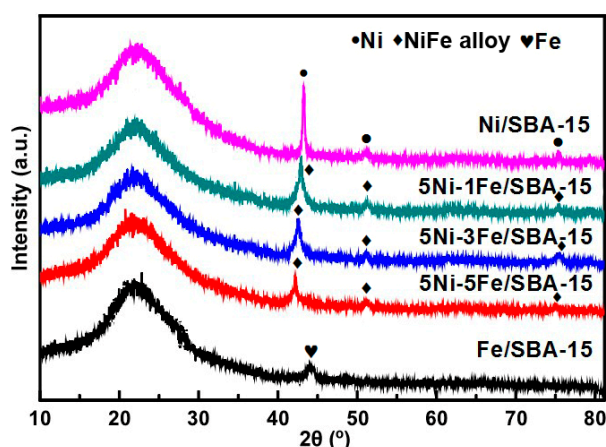


**Figure 1.** XRD (X-ray powder diffraction) patterns of the Ni/SBA-15, 5Ni-1Fe/SBA-15, 5Ni-3Fe/SBA-15, 5Ni-5Fe/SBA-15, and Fe/SBA-15 catalysts.

TEM characterization of the synthesized catalysts was carried out to better investigate their textural properties. As shown in Figure 2, Ni particles (black spots) are quite well dispersed on the porous SBA-15 support. For Ni/SBA-15, the average Ni particle size is about 20 nm, which is in

agreement with data in the literature [31]. The addition of Fe decreases the average size of Ni particles, which are more uniformly distributed, especially in the case of 5Ni-3Fe/SBA-15 (Ni particle size of about 9 nm), indicating that the Fe doping promotes a more homogeneous Ni dispersion, minimizing the formation of aggregates. However, when both metals are used in the same amount (5:5), the average particle size becomes higher (16 nm), highlighting that the Ni:Fe molar ratio should be carefully tuned. Based on these preliminary characterization data, the optimum achieved Ni:Fe molar ratio is 5:3.

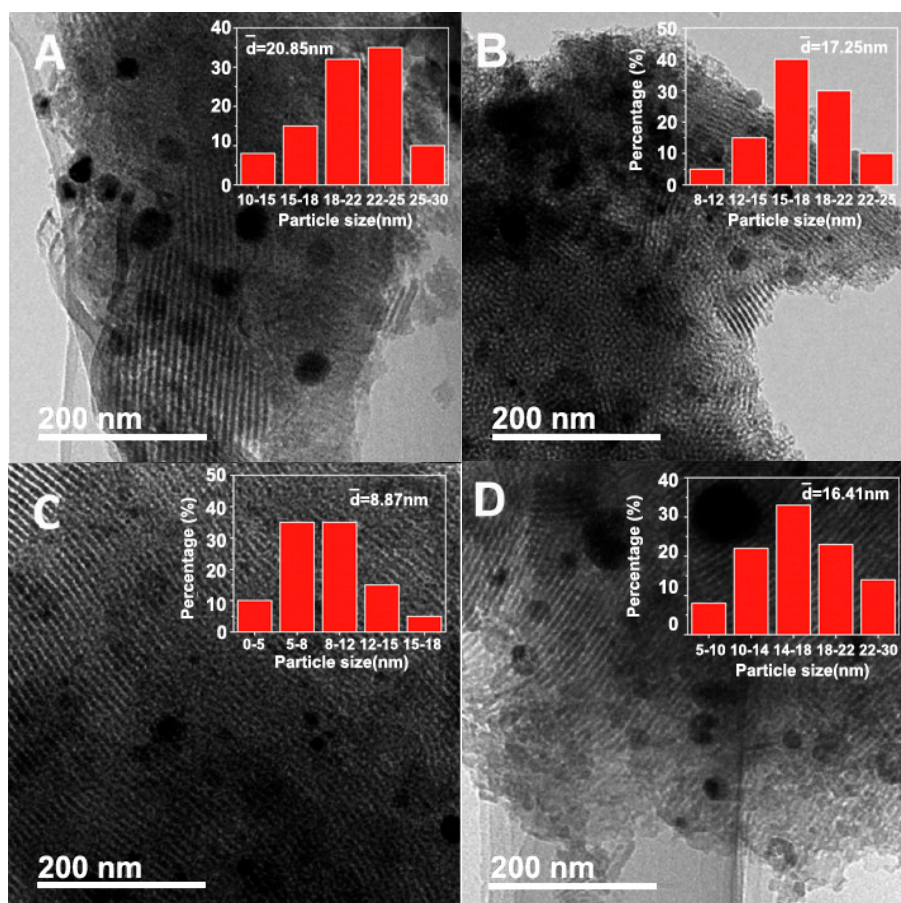


**Figure 2.** TEM (transmission electron microscopy) images of (A) Ni/SBA-15, (B) 5Ni-1Fe/SBA-15, (C) 5Ni-3Fe/SBA-15, and (D) 5Ni-5Fe/SBA-15 catalysts.

To further investigate the interactions between Ni and Fe within the Ni-Fe/SBA-15 catalyst,  $H_2$ -TPR analysis of both monometallic Ni/SBA-15, Fe/SBA-15, and bimetallic Ni-Fe/SBA-15 catalysts, was carried out (Figure 3). For the Ni/SBA-15 catalyst, only one peak was found at 430 °C, due to the reduction of NiO to metallic Ni. For the monometallic Fe/SBA-15 catalyst, three different reduction peaks were detected, at 370, 550, and 630 °C. In this regard, the reduction of  $Fe_2O_3$  to  $\alpha$ -Fe occurs by three consecutive steps:  $Fe_2O_3$ - $Fe_3O_4$ - $FeO$ -Fe [32]. Therefore, the peak at about 370 °C is due to the reduction from  $Fe_2O_3$  to  $Fe_3O_4$ , whilst that from  $Fe_3O_4$  to FeO occurs at about 550 °C, and that at 630 °C corresponds to the reduction from FeO to  $\alpha$ -Fe [32]. Regarding the bimetallic Ni-Fe/SBA-15 catalyst, there are two different peaks between 300 and 550 °C, whilst no peak was found at 600 °C, thus confirming the absence of unalloyed Fe in the synthesized bimetallic catalyst. For 5Ni-1Fe/SBA-15, the reduction peak at 320 °C is assigned to the reduction of  $Fe_2O_3$  to  $Fe_3O_4$ , because  $Fe_2O_3$  is more easily reducible than NiO [33], whilst that at 440 °C is attributed to the reduction of NiO. Compared with the monometallic Ni/SBA-15 catalyst, the reduction peak of the Ni-Fe/SBA-15 catalysts is shifted to higher temperatures, corresponding to the increase of the Fe content, and the  $H_2$  consumption

gradually increases. H<sub>2</sub> may be more easily dissociated and activated on Ni, and then overflowed to the adjacent iron oxide to reduce it, thus leading to the formation of the Ni-Fe alloy [34].

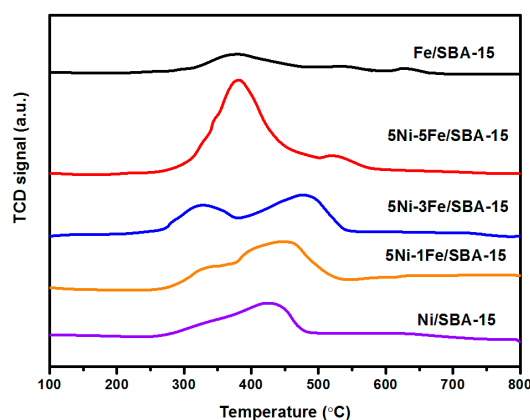


**Figure 3.** H<sub>2</sub>-TPR (hydrogen temperature-programmed reduction) profiles of Ni/SBA-15, 5Ni-1Fe/SBA-15, 5Ni-3Fe/SBA-15, and 5Ni-5Fe/SBA-15 catalysts.

H<sub>2</sub>-TPD profiles of the synthesized catalysts are reported in Figure S2. For Ni/SBA-15, a desorption peak was detected at 100 °C, in agreement with the adsorption of hydrogen on the surface of dispersed metal particles Ni in Figure S2. It is remarkable that the hydrogen desorption peak gradually moves to a higher temperature with the corresponding increase of Fe content. Moreover, the corresponding hydrogen desorption peaks for 5Ni-1Fe/SBA-15 and 5Ni-3Fe/SBA-15 are located at 105 and 125 °C, respectively, which is higher than that of Ni/SBA-15. However, 5Ni-5Fe/SBA-15 has two hydrogen adsorption sites, a low- (150 °C) and high-temperature desorption peak (300 °C), the latter deriving from the hydrogen desorption on the surface of Fe or from the poor dispersion of Ni. In addition, the hydrogen desorption peak from Ni/SBA-15 to 5Ni-5Fe/SBA-15 is shifted to a higher temperature, indicating that the adsorption of hydrogen on the active metal surface is enhanced. The desorption peak of Fe/SBA-15 appears at a higher temperature (250 °C), which is attributed to the hydrogen desorption from the Fe surface. The adsorption center corresponds to the desorption peak at low temperature, and desorption temperature of Fe/SBA-15 is the highest, meaning that the hydrogen desorption from the Fe species requires more energy than that from the Ni ones. To evaluate the dispersion of the particles, the amount of the hydrogen desorbed from the catalyst surface was calculated (Table 1), and it corresponds to the area of the desorption peak reported in Figure S2. The amount of desorbed hydrogen gradually increases with the area of the desorption peak, indicating the increase of the number of active hydrogen on the catalyst surface. With the increase in Fe content, that is moving from 5Ni-1Fe/SBA-15 to 5Ni-3Fe/SBA-15, the particle dispersion increases. However, for the 5Ni-5Fe/SBA-15 catalyst, the total amount of desorbed H<sub>2</sub> does not significantly increase, at the same time showing a worsening of the catalyst dispersion. Moreover, the total acidity of catalysts increases with the amount of Fe. It has been reported that, when Ni is doped with Fe, the unreduced Fe can act as a Lewis acid, thus increasing the acid content of the catalyst [35].

**Table 1.** Chemical properties of the synthesized monometallic Ni/SBA-15, Fe/SBA-15, and bimetallic Ni-Fe/SBA-15 catalysts.

Catalyst	Ni (mmol/g)	Fe (mmol/g)	H <sub>2</sub> (μmol/g) <sup>a</sup>	Particle Dispersion (%) <sup>b</sup>	Total Acidity (μmol/g) <sup>c</sup>
Ni/SBA-15	0.85	0	6.3	1.45	28.3
5Ni-1Fe/SBA-15	0.85	0.17	17.1	3.34	30.6
5Ni-3Fe/SBA-15	0.85	0.50	23.6	3.49	65.2
5Ni-5Fe/SBA-15	0.85	0.86	23.8	2.76	61.5
Fe/SBA-15	0	0.86	14.8	-	78.6

<sup>a</sup>: Amount of H<sub>2</sub> desorption calculated by TPD (Figure S2). <sup>b</sup>: H/(Ni + Fe) ratio. <sup>c</sup>: calculated by NH<sub>3</sub>-TPD.

XPS analysis was performed to monitor the change of the oxidation state of the bimetallic catalysts. The XPS patterns of Ni 2p and Fe 2p of 5Ni/SBA-15, 5Ni-1Fe/SBA-15, 5Ni-3Fe/SBA-15, 5Ni-5Fe/SBA-15, and 5Fe/SBA-15 are shown in Figure S1, respectively. For the Ni 2p, Ni 2p<sub>3/2</sub> and 2p<sub>1/2</sub> spin orbit doublets were deconvoluted into six peaks within the range 845–885 eV (Figure S1a). For the 5Ni/SBA-15 catalyst, the peaks at 853.2, 856.7, and 861.7 eV are assigned to the characteristic peaks of Ni<sup>0</sup>, Ni<sup>2+</sup>, and satellite peaks of Ni<sup>2+</sup> in Ni 2p<sub>3/2</sub> orbit, respectively [8]. For 5Ni-1Fe/SBA-15, 5Ni-3Fe/SBA-15, and 5Ni-5Fe/SBA-15 catalysts, the characteristic peaks of Ni<sup>0</sup>, Ni<sup>2+</sup>, and satellite peaks of Ni<sup>2+</sup> in Ni 2p<sub>3/2</sub> orbit are progressively shifted to the higher binding energies, respectively, indicating a deeper interaction between Ni and Fe. In detail, the electrons are transferred from the oxophilic site of Fe to Ni, increasing the electron density of the outer layer of Ni, in agreement with the literature [36]. Moreover, the characteristic peaks of 5Ni-3Fe/SBA-15 are shifted greatly (0.6 eV), meaning that the reduction of 5Ni-3Fe/SBA-15 is certainly favored. For the Fe 2p in Figure S1b, two spin orbits are also present as Fe 2p<sub>3/2</sub> and Fe 2p<sub>1/2</sub>. For the Fe/SBA-15 catalyst, the peaks at 707.7, 712.2, and 716.4 eV are assigned to Fe<sup>0</sup>, Fe<sup>2+</sup>, and Fe<sup>3+</sup> on Fe 2p<sub>3/2</sub>, respectively [37]. For 5Ni-1Fe/SBA-15, 5Ni-3Fe/SBA-15, and 5Ni-5Fe/SBA-15 catalysts, the characteristic peaks of Fe<sup>0</sup> and Fe<sup>3+</sup> are shifted towards the low binding energies, respectively, indicating that the electrons are indeed obtained by Fe, decreasing the electron density of the outer layer of Fe, and activating the C=O bond. From the XPS results, it can be concluded that the Lewis acid sites of the catalysts derive from the unsaturated coordination of Fe<sup>2+</sup> and Fe<sup>3+</sup> ions. Moreover, the characteristic peak area of Fe<sup>0</sup> in bimetallic Ni-Fe catalyst increases, indicating that the interaction between Ni and Fe promotes the reduction of iron oxide. The above results confirm that 5Ni-3Fe/SBA-15 is the most promising catalyst to test for the activation of the C=O bond of LA.

## 2.2. LA to GVL Catalytic Tests

Preliminary catalytic tests were carried out to test the effectiveness of the synthesized catalysts towards GVL production. First, GC-MS analysis was carried out to monitor the progress of the reaction (Figure S4). This analysis confirms that methyl levulinate and GVL represent the main intermediate and target product, respectively, indicating that LA could be completely hydrogenated to GVL, by properly tuning the reaction conditions. In this regard, 4-hydroxyvaleric acid, which is the intermediate of interest for the MPV intermolecular hydrogenation mechanism (path B, Scheme 2), was not detected in the reaction mixture. In principle, LA is firstly adsorbed on the surface of the catalyst and subsequently esterified with methanol (MeOH) to methyl levulinate, benefiting from the Lewis acidity of the catalyst [22]. To investigate the mechanism of LA adsorption on the catalysts, in situ FT-IR analysis was performed. As shown in Figure 4, the LA absorption band in the range 1750–1765 cm<sup>-1</sup> is instead absent in Ni/SBA-15 and Ni-Fe/SBA-15, meaning that the physical adsorption of LA on these catalysts is weak. Moreover, in the case of the Ni/SBA-15 catalyst, an absorption band at about 1720 cm<sup>-1</sup> was detected, due to the weak chemical adsorption of C=O stretching vibration of LA, indicating an interaction between the cationic or Lewis acid sites on the surface of Ni/SBA-15 catalyst and the lone pair electron of the carbonyl oxygen of LA [38]. In contrast, no absorption

band was found at  $1720\text{ cm}^{-1}$  for 5Ni-3Fe/SBA-15, whilst a blue shift occurs in the range  $1650\text{--}1680\text{ cm}^{-1}$ , which is due to the strong LA chemisorption. The oxophilic promoter of Fe rendered more Lewis active sites for acid adsorption the C=O bond, in agreement with the results of XPS and  $\text{NH}_3$ -TPD characterization. Moreover, the composition of the gas phase was investigated to highlight possible differences between the catalysts towards the potential production of hydrogen (Figure S3). These analyses confirm that  $\text{H}_2$  and  $\text{CO}_2$  are the main reaction products of the gas phase. However, for the Ni/SBA-15 catalyst, the  $\text{H}_2$  selectivity is only 40 mol %, whilst, in the case of 5Ni-3Fe/SBA-15, the addition of Fe significantly improves the  $\text{H}_2$  selectivity up to 90 mol %. Instead, regarding the 5Ni-5Fe/SBA-15 catalyst,  $\text{H}_2$  selectivity decreases, probably as a consequence of the larger particle size of Ni, according to the results of the above-discussed characterization.

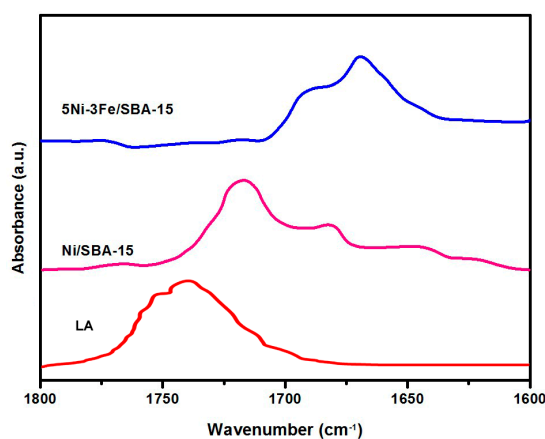


**Figure 4.** In situ FT-IR (Fourier transform–infrared spectroscopy) spectrum of LA and LA absorption on Ni/SBA-15 and 5Ni-3Fe/SBA-15 ( $50\text{ mL}\cdot\text{min}^{-1}$  He, at  $200\text{ }^\circ\text{C}$ , 2 h).

The effect of temperature, reaction time, and hydrogen source on the LA hydrogenation to GVL was investigated. Figure 5a shows that the temperature has an important role on the LA conversion and GVL selectivity. Going from  $50$  to  $100\text{ }^\circ\text{C}$ , both LA conversion and GVL selectivity are low, whilst the catalytic performances significantly improve at  $150\text{ }^\circ\text{C}$  and, even better, at  $200\text{ }^\circ\text{C}$ . LA is not immediately hydrogenated into the corresponding alcohol, and methyl levulinate is the only detected intermediate, whilst GVL is subsequently produced by cyclization and dealcoholation mechanisms [39]. The effect of the reaction time was also considered (Figure 5b). The LA conversion is almost complete after only 30 min, and GVL selectivity rapidly increases from 30 to 120 min, becoming complete after 180 min. Lastly, the effect of the hydrogen source was preliminarily investigated by comparing the effect of molecular hydrogen and MeOH for the GVL production, in the absence/presence of the bimetallic 5Ni-3Fe/SBA-15 catalyst (Figure 5c). The LA conversion in MeOH is slightly higher than that obtained with molecular hydrogen. Remarkably, the GVL selectivity is significantly higher for the catalytic tests carried out in the presence of MeOH, thus confirming the positive synergism achieved thanks to the combined use of the bimetallic Fe-Ni catalyst and MeOH for promoting the selective hydrogenation of the C=O bond. These preliminary data confirm that the catalytic performances of the synthesized catalysts are comparable with those of noble metal catalysts, such as ruthenium, which has been identified as a very efficient catalyst for GVL production. For example, Xiao et al. reported an almost complete LA conversion (99.7 mol %) and a complete selectivity towards GVL, adopting a batch reactor, in the presence of Ru/graphene catalyst ( $40\text{ bar H}_2$ ,  $200\text{ }^\circ\text{C}$ , 8 h) [40]. Piskun et al. found a maximum LA conversion of 90 mol %, but a low selectivity (66 mol % of GVL), using Ru/Beta-12.5 ( $45\text{ Bar H}_2$ ,  $90\text{ }^\circ\text{C}$ , 2 h) [41]. Luo et al. reported a maximum GVL selectivity of 97.5 mol % at complete LA conversion, adopting Ru/ $\text{TiO}_2$  as a catalyst, and dioxane as the reaction medium ( $4\text{ MPa H}_2$ ,  $200\text{ }^\circ\text{C}$ , 4 h) [42]. However, in all these mentioned cases, pentanoic acid was identified as a reaction by-product, this compound deriving from the GVL ring opening, a reaction catalyzed by highly acidic supports [25].

Instead, in our case, pentanoic acid was not produced, thanks to the milder acidity of the adopted catalyst, leading to a more selective production of the desired GVL.

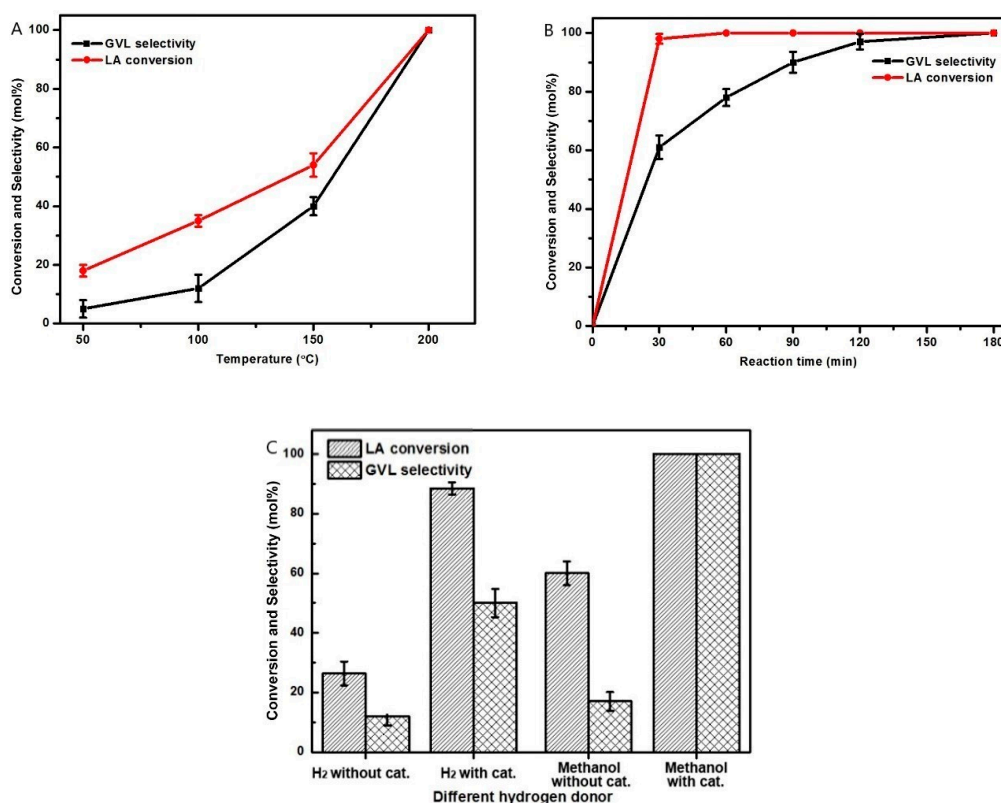


**Figure 5.** (A) The effect of temperature (reaction conditions: 2 g LA, 15 mL MeOH, 0.5 g 5Ni-3Fe/SBA-15, 180 min), (B) reaction time (reaction conditions: 2 g LA, 15 mL methanol, 0.5 g 5Ni-3Fe/SBA-15, 200 °C) and (C) different hydrogen sources (H<sub>2</sub> and MeOH) (reaction conditions: 2 g LA, 1 MPa H<sub>2</sub> or 15 mL MeOH, 0.5 g 5Ni-3Fe/SBA-15, 200 °C, 180 min) on LA conversion and GVL selectivity.

Preliminary recycling tests of the most promising bimetallic catalyst (5Ni-3Fe/SBA-15) were carried out to demonstrate its stability (Figure 6). The 5Ni-3Fe/SBA-15 catalyst was re-used consecutively five times under the best-identified reaction conditions. Before each cycle run, the spent catalyst was simply washed with ethanol in an ultrasonic cleaner and dried in a vacuum oven at 60 °C, thus avoiding tedious reactivation procedures. If compared with the performances of the fresh catalyst, those of the spent 5Ni-3Fe/SBA-15 catalyst decrease only slightly, even after five recycling tests, thus confirming the good potential of this catalytic system for GVL production on a larger scale.

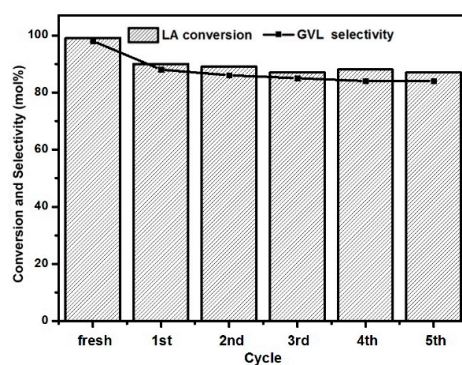


**Figure 6.** Recycling tests of 5Ni-3Fe/SBA-15 catalyst.

### 3. Experimental Section

#### 3.1. Materials

Levulinic acid,  $\gamma$ -valerolactone, and methyl levulinate were purchased by Shanghai Aladdin Reagent Company (Aladdin, Shanghai, China). Nickel(II) nitrate hexahydrate  $[(\text{Ni}(\text{NO}_3)_2 \cdot 6\text{H}_2\text{O})]$ , ferric(III) nitrate hexahydrate  $[\text{Fe}(\text{NO}_3)_3 \cdot 9\text{H}_2\text{O}]$ , dichloromethane (DCM), and MeOH were purchased from Sigma-Aldrich Trading Co., Ltd. (Sigma-Aldrich, Shanghai, China). SBA-15 was produced by Sinopharm Chemical Reagent Co., Ltd. (Sinopharm, Shanghai, China). Double-distilled  $\text{H}_2\text{O}$  was used for the synthesis of catalysts.

#### 3.2. Preparation of Catalyst

The metal-based catalysts were prepared by the incipient wetness impregnation method [21]. Solutions of nickel(II) nitrate hexahydrate and ferric(III) nitrate hexahydrate were mixed in the appropriate molar ratio (nominal weight content of 5 wt% Ni, Ni:Fe molar ratio = 5:0, 5:1, 5:2, 5:5). Then, 1 g of SBA-15 was added into the 10 mL volume of the metal precursor solution. The resulting slurry was stirred at room temperature for 2 h, then the catalyst was recovered, and dried overnight at 120 °C. The calcination was carried out under  $\text{N}_2$  atmosphere at 450 °C (heating rate 5 °C/min) for 1 h and the catalyst was reduced at 450 °C (heating rate 5 °C/min) for 3 h, under  $\text{H}_2$  flow.

#### 3.3. Characterization of the Catalysts

Powder X-ray diffraction (XRD) analysis was carried out by a Rigaku Ultima IV X-ray diffractometer (Rigaku, Tokyo, Japan), utilizing  $\text{Cu-K}\alpha$  radiation ( $\lambda = 1.5405 \text{ \AA}$ ). The test conditions were tube voltage, 50 kV; tube current, 50 mA; scanning speed, 8°/min; and scanning range, 10°–80°.  $\text{N}_2$  sorption measurements were carried out at 77 K on a BEL-MAX gas/vapor adsorption instrument (MicrotracBEL Corp., Osaka, Japan). The surface areas were measured by the Brunauer-Emmett-Teller (BET) method. Transmission electron microscopy (TEM) was performed by the JEM-2100 microscope (JEOL, Tokyo, Japan), working at 200 kV. X-ray photoelectron spectroscopy (XPS) characterization was carried out by a Scientific Escalab 250 spectrometer (Thermo, Waltham, MA, USA) with  $\text{AlK}\alpha$  ( $h\nu = 1486.6 \text{ eV}$ ) radiation, at a pressure of about  $1 \times 10^{-9}$  Torr. The binding energy values were corrected by using the  $\text{C1s}$  peak (284.6 eV). The total acidity was determined by  $\text{NH}_3$ -TPD technique. The calcined samples were characterized using temperature-programmed reduction by a TP-5080 adsorption instrument (xq-instrument, Tianjin, China), which was equipped with a TCD detector. Hydrogen temperature-programmed desorption ( $\text{H}_2$ -TPD) measurements were performed by an Autochem II-2920 (Norcross, GA, USA) instrument. The total  $\text{H}_2$  desorption was calculated by measuring the areas of the desorption peaks. The FT-IR spectra were acquired by a Nicolet NEXUS 670 (Thermo, Waltham, MA, USA), which was equipped with an in situ IR cell.

#### 3.4. Catalytic Tests

The catalytic hydrogenation of LA was carried out in a 100-mL stainless steel batch autoclave (Parr, Moline, IL, USA). In a typical run, the autoclave was loaded with the catalyst (0.5 g), LA (2 g), and MeOH (15 mL). Then, the reactor was heated up to the set-point temperature, under a constant stirring rate of 1000 rpm. At the end of the reaction, the slurry was recovered and centrifuged to separate the liquid phase from the spent catalyst, and the former was further analyzed by GC-MS and GC-FID techniques.

#### 3.5. Analysis of the Liquid Phase

Qualitative analysis of the liquid samples was carried out by a GCMS-QP2010 instrument (Shimadzu, Kyoto, Japan), equipped with an RTX-5MS column (30 m  $\times$  0.25 mm  $\times$  0.25  $\mu\text{m}$ ). The injector temperature was 250 °C and a split ratio of 20:1 was employed. The MS operated in EI mode at

70 eV and the ion source temperature was set at 230 °C. The temperature program was the following: from 50 °C to 250 °C at a heating rate of 10 °C/min and held for 5 min at 250 °C. He was the carrier gas, and a column flow of 1.0 mL/min was used. The quantitative analysis was carried out by a GC-2010 gas-chromatograph (Shimadzu, Kyoto, Japan), equipped with an RTX-50 column (30 m × 0.25 mm × 0.25 µm) and a flame ionization detector. *n*-dodecane was used as the internal standard. Conversion and selectivity parameters were calculated according to the following equations:

$$\text{Conversion of LA (mol \%)} = \left(1 - \frac{n_{LA \text{ final}}}{n_{LA \text{ initial}}}\right) * 100 \text{ mol \%} \quad (1)$$

$$\text{Selectivity to GVL (mol \%)} = \frac{n_{GVL}}{n_{products}} * 100 \text{ mol \%} \quad (2)$$

#### 4. Conclusions

γ-valerolactone is an important biomass platform molecule that can be used as a biofuel, pharmaceutical intermediate, food additive, and green solvent. The conversion of levulinic acid into high-value-added γ-valerolactone is an important reaction, and still requires the development of cheap and highly effective catalysts. In this regard, this paper is mainly focused on the synthesis of new Ni-Fe/SBA-15 bimetallic catalysts for improving the hydrogenation of levulinic acid into γ-valerolactone, adopting methanol as the only hydrogen donor. The physicochemical properties of the synthesized bimetallic catalysts were investigated by different techniques, e.g., XRD, TEM, XPS, and H<sub>2</sub>-TPD. H<sub>2</sub>-TPD confirmed that the addition of Fe as an oxophilic promoter lowers the reduction temperature of the NiO phase and improves the reducibility of the mixed oxides. At the same time, the presence of Fe favorably increased the Lewis acidity, which is beneficial for the MPV reduction of LA to GVL. Moreover, XPS analysis confirmed an electronic transfer from Fe to Ni, promoting the activation of the C=O bond of LA, and this conclusion is in agreement with the in situ FT-IR characterization. The preliminary catalytic tests have shown that the best bimetallic 5Ni-3Fe/SBA-15 catalyst has promising performances towards GVL synthesis. The effect of temperature and reaction time on GVL production was also considered, achieving complete LA conversion and GVL selectivity, working at 200 °C and after 180 min. Lastly, preliminary recycling tests of the best performing Ni-Fe bimetallic catalyst confirmed the possibility of its advantageous re-use, achieving satisfactory performances to γ-valerolactone, even after five catalytic cycles. The good catalytic performances/stability, the low cost, and the easy synthesis/regeneration of our Ni-Fe bimetallic catalysts are key aspects for the real development of γ-valerolactone production on a larger scale, thus filling the still existing gap between the industrial and academic world.

**Supplementary Materials:** The following are available online at <http://www.mdpi.com/2073-4344/10/9/1096/s1>. Figure S1: XPS profiles of reduced catalysts. Figure S2: H<sub>2</sub>-TPD profiles of the synthesized SBA-15 supported catalysts. Figure S3: Influence of metals supported with SBA-15 on the amount of hydrogen in gas. Figure S4: GC-MS results for hydrogenation of LA with different reaction times.

**Author Contributions:** Conceptualization, L.L.; methodology, Q.Z. and X.H.; analysis, L.L., Q.Z. and X.H.; writing, original draft preparation, X.H. and Q.Z.; writing, review and editing, L.L.; project administration, L.L. All authors have read and agreed to the published version of the manuscript.

**Funding:** This work is supported by the National Natural Science Foundation of China (Grant No.31801321), and sponsored by Shanghai Sailing Program (Grant No. 19YF1436300) and Natural Science Foundation of Shanghai (Grant No. 18ZR1428100).

**Conflicts of Interest:** The authors declare no conflict of interest.

## References

1. Climent, M.J.; Corma, A.; Iborra, S. Conversion of biomass platform molecules into fuel additives and liquid hydrocarbon fuels. *Green Chem.* **2014**, *16*, 516–547. [[CrossRef](#)]
2. Zhu, C.; Wang, H.L.Q.; Wang, C.; Xu, Y.; Zhang, Q.; Ma, L. Chapter 3-5-hydroxymethyl furfural-a C<sub>6</sub> precursor for fuels and chemicals. In *Biomass, Biofuels, Biochemicals*; Saravanamurugan, S., Pandey, A., Li, H., Riisager, A., Eds.; Elsevier: Amsterdam, The Netherlands, 2020; pp. 61–94. [[CrossRef](#)]
3. Kang, S.; Fu, J.; Zhang, G. From lignocellulosic biomass to levulinic acid: A review on acid-catalyzed hydrolysis. *Renew. Sustain. Energy Rev.* **2018**, *94*, 340–362. [[CrossRef](#)]
4. Molinari, V.; Antonietti, M.; Esposito, D. An integrated strategy for the conversion of cellulosic biomass into  $\gamma$ -valerolactone. *Catal. Sci. Technol.* **2014**, *4*, 3626–3630. [[CrossRef](#)]
5. Tang, X.; Sun, Y.; Zeng, X.; Lei, T.; Li, H.; Lin, L.  $\gamma$ -Valerolactone—An excellent solvent and a promising building block. In *Biomass, Biofuels, Biochemicals*; Saravanamurugan, S., Pandey, A., Li, H., Riisager, A., Eds.; Elsevier: Amsterdam, The Netherlands, 2020; pp. 199–226. [[CrossRef](#)]
6. Ye, L.; Han, Y.; Feng, J.; Lu, X. A review about GVL production from lignocellulose: Focusing on the full components utilization. *Ind. Crops Prop.* **2020**, *144*, 112031. [[CrossRef](#)]
7. Alonso, D.M.; Wettstein, S.G.; Dumesic, J.A. Gamma-valerolactone, a sustainable platform molecule derived from lignocellulosic biomass. *Green Chem.* **2013**, *15*, 584–595. [[CrossRef](#)]
8. Yan, Z.; Lin, L.; Liu, S. Synthesis of  $\gamma$ -valerolactone by hydrogenation of biomass-derived levulinic acid over Ru/C catalyst. *Energy Fuel* **2009**, *23*, 3853–3858. [[CrossRef](#)]
9. Manzer, L.E. Catalytic synthesis of  $\alpha$ -methylene- $\gamma$ -valerolactone: A biomass-derived acrylic monomer. *Appl. Catal. A Gen.* **2004**, *272*, 249–256. [[CrossRef](#)]
10. Son, P.A.; Nishimura, S.; Ebitani, K. Production of  $\gamma$ -valerolactone from biomass derived compounds using formic acid as a hydrogen source over supported metal catalysts in water solvent. *RSC Adv.* **2014**, *4*, 10525. [[CrossRef](#)]
11. Upare, P.P.; Lee, J.; Hwang, D.; Halligudi, S.B.; Hwang, Y.; Chang, J. Selective hydrogenation of levulinic acid to  $\gamma$ -valerolactone over carbon-supported noble metal catalysts. *J. Ind. Eng. Chem.* **2011**, *17*, 287–292. [[CrossRef](#)]
12. Deng, L.; Zhao, Y.; Li, J.; Fu, Y.; Liao, B.; Guo, Q. Conversion of levulinic acid and formic acid into  $\gamma$ -valerolactone over heterogeneous catalysts. *ChemSusChem* **2010**, *3*, 1172–1175. [[CrossRef](#)]
13. Yu, Z.; Lu, X.; Bai, H.; Xiong, J.; Feng, W.; Ji, N. Effects of solid acid supports on the bifunctional catalysis of levulinic acid to  $\gamma$ -valerolactone: Catalytic activity and stability. *Chem. Asian J.* **2020**, *15*, 1182–1201. [[CrossRef](#)] [[PubMed](#)]
14. Dutta, S.; Yu, I.K.M.; Tsang, D.C.W.; Ng, Y.H.; Ok, Y.S.; Sherwood, J.; Clark, J.H. Green synthesis of gamma-valerolactone (GVL) through hydrogenation of biomass-derived levulinic acid using non-noble metal catalysts: A critical review. *Chem. Eng. J.* **2019**, *372*, 992–1006. [[CrossRef](#)]
15. Mohan, V.; Venkateswarlu, V.; Pramod, C.V.; Raju, B.D.; Rao, K.S.R. Vapour phase hydrocyclisation of levulinic acid to  $\gamma$ -valerolactone over supported Ni catalysts. *Catal. Sci. Technol.* **2014**, *4*, 1253–1259. [[CrossRef](#)]
16. Galletti, A.M.R.; Antonetti, C.; De Luise, V.; Martinelli, M. A sustainable process for the production of  $\gamma$ -valerolactone by hydrogenation of biomass-derived levulinic acid. *Green Chem.* **2012**, *14*, 688–694. [[CrossRef](#)]
17. Shimizu, K.; Kanno, S.; Kon, K. Hydrogenation of levulinic acid to  $\gamma$ -valerolactone by Ni and MoO<sub>x</sub> co-loaded carbon catalysts. *Green Chem.* **2014**, *16*, 3899–3903. [[CrossRef](#)]
18. Obregón, I.; Corro, E.; Izquierdo, U.; Requies, J.; Arias, P.L. Levulinic acid hydrogenolysis on Al<sub>2</sub>O<sub>3</sub>-based Ni-Cu bimetallic catalysts. *Chin. J. Catal.* **2014**, *35*, 656–662. [[CrossRef](#)]
19. Zhou, X.; Huang, Y.; Xing, W.; Liu, C.; Liao, J.; Lu, T. High-quality hydrogen from the catalyzed decomposition of formic acid by Pd- Au/C and Pd-Ag/C. *Chem. Commun.* **2008**, 3540–3542. [[CrossRef](#)] [[PubMed](#)]
20. Fellay, C.; Yan, N.; Dyson, P.J.; Laurency, G. Selective formic acid decomposition for high-pressure hydrogen generation: A mechanistic study. *Chem. Eur. J.* **2009**, *15*, 3752–3760. [[CrossRef](#)]
21. Ruppert, A.M.; Sneká-Płatek, O.; Jędrzejczyk, M.; Keller, N.; Dumon, A.S.; Michel, C.; Sautet, P.; Grams, J. Ru catalysts for levulinic acid hydrogenation with formic acid as a hydrogen source. *Green Chem.* **2016**, *18*, 2014–2028. [[CrossRef](#)]

22. Yu, Z.; Lu, X.; Bai, H.; Xiong, J.; Feng, W.; Ji, N. Heterogeneous catalytic hydrogenation of levulinic acid to  $\gamma$ -valerolactone with formic acid as internal hydrogen source: Key issues and their effects. *Chemsuschem* **2020**, *13*, 2916–2930. [[CrossRef](#)]
23. Chia, M.; Dumesic, J.A. Liquid-phase catalytic transfer hydrogenation and cyclization of levulinic acid and its esters to gamma-valerolactone over metal oxide catalysts. *Chem. Commun.* **2011**, *47*, 12233–12235. [[CrossRef](#)] [[PubMed](#)]
24. Gilkey, M.J.; Xu, B. Heterogeneous catalytic transfer hydrogenation as an effective pathway in biomass upgrading. *ACS Catal.* **2016**, *6*, 1420–1436. [[CrossRef](#)]
25. Luo, H.Y.; Consoli, D.F.; Gunther, W.R.; Román-Leshkov, Y. Investigation of the reaction kinetics of isolated Lewis acid sites in Beta zeolites for the Meerwein-Ponndorf-Verley reduction of methyl levulinate to  $\gamma$ -valerolactone. *J. Catal.* **2014**, *320*, 198–207. [[CrossRef](#)]
26. Tang, X.; Zeng, X.; Li, Z.; Li, W.; Jiang, Y.; Hu, L.; Liu, S.; Sun, Y.; Lin, L. In Situ generated catalyst system to convert biomass-derived levulinic acid to  $\gamma$ -Valerolactone. *Chemcatchem* **2015**, *7*, 1372–1379. [[CrossRef](#)]
27. Yi, Y.; Liu, H.; Xiao, L.; Wang, B.; Song, G. Highly efficient hydrogenation of levulinic acid into  $\gamma$ -valerolactone using an iron pincer complex. *Chemsuschem* **2018**, *9*, 1474–1478. [[CrossRef](#)] [[PubMed](#)]
28. Li, M.; Wei, J.; Yan, G.; Liu, H.; Tang, X.; Sun, Y.; Zeng, X.; Lei, T.; Lin, L. Cascade conversion of furfural to fuel bioadditive ethyl levulinate over bifunctional zirconium-based catalysts. *Renew. Energy* **2020**, *147*, 916–923. [[CrossRef](#)]
29. Norhasyimi, R.; Ahmad, Z.A.; Abdullah, R.M. A Review: Mesoporous santa barbara amorphous-15, types, synthesis and its applications towards biorefinery production. *Am. J. Appl. Sci.* **2010**, *7*, 1579–1586. [[CrossRef](#)]
30. Oyama, S.T.; Zhao, H.; Freund, H.J.; Asakura, K.; Włodarczyk, R.; Sierka, M. Unprecedented selectivity to the direct desulfurization (DDS) pathway in a highly active FeNi bimetallic phosphide catalyst. *J. Catal.* **2012**, *285*, 1–5. [[CrossRef](#)]
31. Jie, F.; Dong, S.; Lu, X. Hydrogenation of levulinic acid over nickel catalysts supported on aluminum oxide to prepare  $\gamma$ -valerolactone. *Catalysts* **2016**, *6*, 6. [[CrossRef](#)]
32. Hsu, P.; Jiang, J.; Lin, Y. Does a strong oxophilic promoter enhance direct deoxygenation? A study of NiFe, NiMo, and NiW catalysts in p-Cresol conversion. *ACS Sustain. Chem. Eng.* **2018**, *6*, 660–667. [[CrossRef](#)]
33. Ren, J.; Qin, X.; Yang, J.; Qin, Z.; Guo, H.; Lin, J.; Li, Z. Methanation of carbon dioxide over Ni-M/ZrO<sub>2</sub> (M=Fe, Co, Cu) catalysts: Effect of addition of a second metal. *Fuel Process. Technol.* **2015**, *137*, 204–211. [[CrossRef](#)]
34. Daniel, T.; José, L.P.; Isabel, S. Co-, Cu- and Fe-doped Ni/Al<sub>2</sub>O<sub>3</sub> catalysts for the catalytic decomposition of methane into hydrogen and carbon nanofibers. *Catalysts* **2018**, *8*, 300. [[CrossRef](#)]
35. Nie, L.; Souza, P.M.D.; Noronha, F.B.; An, W.; Sooknoi, T.; Resasco, D.E. Selective conversion of m-cresol to toluene over bimetallic Ni-Fe catalysts. *J. Mol. Catal. A Chem.* **2014**, *388–389*, 47–55. [[CrossRef](#)]
36. Kumar, V.V.; Naresh, G.; Sudhakar, M.; Tardio, J.; Bhargava, S.K.; Venugopal, A. Role of brønsted and lewis acid sites on Ni/TiO<sub>2</sub> catalyst for vapour phase hydrogenation of levulinic acid: Kinetic and mechanistic study. *Appl. Catal. A Gen.* **2015**, *505*, 217–223. [[CrossRef](#)]
37. Kordulis, C.; Bourikas, K.; Gousi, M. Development of nickel based catalysts for the transformation of natural triglycerides and related compounds into green diesel: A critical review. *Appl. Catal. B Environ.* **2016**, *181*, 156–196. [[CrossRef](#)]
38. Ali, A.; Li, B.; Lu, Y.; Zhao, C. Highly selective and low-temperature hydrothermal conversion of natural oils to fatty alcohols. *Green Chem.* **2019**, *21*, 3059–3064. [[CrossRef](#)]
39. Nadgeri, J.M.; Hiyoshi, N.; Yamaguchi, A.; Sato, O.; Shirai, M. Liquid phase hydrogenation of methyl levulinate over the mixture of supported ruthenium catalyst and zeolite in water. *Appl. Catal. A Gen.* **2014**, *470*, 215–220. [[CrossRef](#)]
40. Xiao, C.; Goh, T.W.; Qil, Z.; Goes, S.; Brashler, K.; Perez, C.; Huang, W. Conversion of levulinic acid to  $\gamma$ -valerolactone over few-layer graphene-supported ruthenium catalysts. *ACS Catal.* **2016**, *6*, 593–599. [[CrossRef](#)]

41. Piskun, A.; Winkelman, J.G.M.; Tang, Z.; Heeres, H.J. Support screening studies on the hydrogenation of levulinic acid to  $\gamma$ -valerolactone in water using Ru catalysts. *Catalysts* **2016**, *6*, 131. [[CrossRef](#)]
42. Luo, W.; Deka, U.; Beale, A.M.; van Eck, E.R.H.; Bruijninx, P.C.A.; Weckhuysen, B.M. Ruthenium-catalyzed hydrogenation of levulinic acid: Influence of the support and solvent on catalyst selectivity and stability. *J. Catal.* **2013**, *301*, 175–186. [[CrossRef](#)]



© 2020 by the authors. Licensee MDPI, Basel, Switzerland. This article is an open access article distributed under the terms and conditions of the Creative Commons Attribution (CC BY) license (<http://creativecommons.org/licenses/by/4.0/>).